Lecture Notes in Electrical Engineering 268

Corrado Di Natale
Vittorio Ferrari
Andrea Ponzoni
Giorgio Sberveglieri
Marco Ferrari
Editors

Sensors and Microsystems

Proceedings of the 17th National Conference, Brescia, Italy, 5-7 February 2013

Springer

Lecture Notes in Electrical Engineering

Volume 268

For further volumes:
http://www.springer.com/series/7818

Corrado Di Natale • Vittorio Ferrari
Andrea Ponzoni • Giorgio Sberveglieri
Marco Ferrari
Editors

Sensors and Microsystems

Proceedings of the 17th National Conference,
Brescia, Italy, 5-7 February 2013

Springer

Editors
Corrado Di Natale
Department of Electronic Engineering
University of Rome Tor Vergata
Rome, Italy

Vittorio Ferrari
Department of Information Engineering
University of Brescia
Brescia, Italy

Andrea Ponzoni
SENSOR Laboratory, IDASC
National Research Council (CNR)
Brescia, Italy

Giorgio Sberveglieri
Department of Information Engineering
University of Brescia
Brescia, Italy

Marco Ferrari
Department of Information Engineering
University of Brescia
Brescia, Italy

ISSN 1876-1100 ISSN 1876-1119 (electronic)
ISBN 978-3-319-00683-3 ISBN 978-3-319-00684-0 (eBook)
DOI 10.1007/978-3-319-00684-0
Springer Cham Heidelberg New York Dordrecht London

Library of Congress Control Number: 2013953711

Printed on acid-free paper

Springer is part of Springer Science+Business Media (www.springer.com)

Contents

Part I
Physical Sensors

Investigation of Seebeck Effect in Metal Oxide Nanowires for Powering Autonomous Microsystems

Simone Dalola, Vittorio Ferrari, Guido Faglia, Elisabetta Comini, Matteo Ferroni, Caterina Soldano, Dario Zappa, and Giorgio Sberveglieri

1 Introduction

Quasi-monodimensional metal oxide nanostructures have been recently considered as promising candidates to develop high-efficiency and high-temperature thermoelectric devices due to their reduced dimensionality and excellent durability at high temperature [1]. The fabrication of a thermoelectric generator (TEG) requires both *n*- and *p*-type elements. To this purpose, bundles of ZnO (*n*-type) and CuO (*p*-type) nanowires have been grown by thermal evaporation process [2] and thermal oxidation techniques [3], respectively, and a planar thermoelectric generator has been fabricated.

2 Material Preparation

The deposition technique for zinc oxide nanowires consists in the thermally driven evaporation of a powder of bulk metal oxides followed by condensation on a substrate in an alumina tubular furnace capable to reach high temperatures (≈1,500 °C), needed to initiate the decomposition and the evaporation of metal oxide powder [2]. The nanowires have been fabricated on alumina 20 × 20 mm^2 substrates with Au nanoparticles deposited by RF sputtering as catalyst.

S. Dalola (✉) • V. Ferrari
Dipartimento di Ingegneria dell'Informazione, Università degli Studi di Brescia, Via Branze 38, 25123 Brescia, Italy
e-mail: simone.dalola@ing.unibs.it

G. Faglia • E. Comini • M. Ferroni • C. Soldano • D. Zappa • G. Sberveglieri
SENSOR Lab, Università degli Studi di Brescia and CNR-IDASC, Via Valotti 9, 25133 Brescia, Italy

C. Di Natale et al. (eds.), *Sensors and Microsystems: Proceedings of the 17th National Conference, Brescia, Italy, 5-7 February 2013*, Lecture Notes in Electrical Engineering 268, DOI 10.1007/978-3-319-00684-0_1,

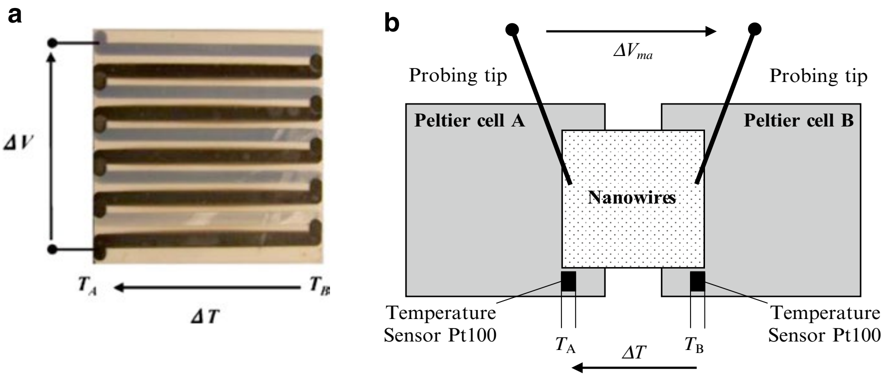

Fig. 1 (**a**) Picture of the fabricated planar TEG. (**b**) Schematic diagram of the experimental setup for the measurement of the thermoelectric response of nanowires samples

Copper oxide nanowires have been grown by thermal oxidation of metallic Cu thin film layer, previously deposited by RF magnetron sputtering on 20×20 mm^2 alumina substrates [3].

By combining *n*- and *p*-type nanostructured elements, a planar TEG consisting of five ZnO and CuO thermocouples, electrically connected in series and thermally in parallel, has been designed and fabricated. Thermoelectric material depositions have been patterned via shadow mask technique on alumina 20×20 mm^2 substrates to form an array of elements. Each element consists of an *S*-shaped strip 20 mm in length and 1 mm in width. The electrical contact is provided by the overlap of adjacent strips. ZnO nanowires have been grown by thermal evaporation technique before copper deposition, to avoid contaminations; then the entire device has been oxidized in a furnace. A top-view picture of the planar thermoelectric generator is shown in Fig. 1a.

3 Measurement of the Thermoelectric Response

The thermoelectric response of the fabricated samples has been experimentally investigated by measuring the thermoelectric voltage as a function of the temperature difference $\Delta T = T_A - T_B$ applied by means of an experimental setup, based on two Peltier cells, which provides the temperatures T_A and T_B at the edges of the sample, as shown in Fig. 1b.

The thermoelectric voltages on the ZnO and CuO nanowire bundles have been measured by means of a pair of Chromel probes, which connect the nanowire bundle to the electronic measurement unit [4]. The voltage ΔV, measured at the tips, is proportional to the temperature difference ΔT as follows:

$$\Delta V = \alpha_{m,Ch}\Delta T = \left(\alpha_m - \alpha_{Ch}\right)\Delta T \tag{1}$$

where $\alpha_{m,\mathrm{Ch}}$ is the Seebeck coefficient of the tested material (ZnO or CuO) labelled m, with respect to the reference material Ch, i.e., Chromel, while α_m and $\alpha_{\mathrm{Ch}} = 28.1$ μV/°C [5] are the absolute Seebeck coefficients of the tested material m and the Chromel, respectively.

For the characterization of the planar thermoelectric generator, the thermoelectric voltage ΔV has been measured using a pair of copper probing tips by means of the above-described experimental setup, as a function of the applied temperature difference ΔT. The thermoelectric voltage ΔV provided by the TEG is proportional to the applied temperature difference ΔT by means of the Seebeck coefficient S of the entire thermoelectric device, as it follows:

$$\Delta V = S\Delta T = N\alpha_{CuO,ZnO}\Delta T = N\left(\alpha_{CuO} - \alpha_{ZnO}\right)\Delta T \tag{2}$$

where $N = 5$ and $\alpha_{\mathrm{Cuo,ZnO}}$ are the number and the Seebeck coefficient of the ZnO–CuO thermocouples composing the thermoelectric device, respectively.

The voltage ΔV has been amplified by means of a low-noise instrumentation amplifier INA111 with a gain of 100 for the characterization of both metal oxide nanowires and planar thermoelectric generator.

4 Experimental Results

Figure 2a shows the applied temperature difference ΔT and the corresponding thermoelectric voltage ΔV measured for a ZnO nanowire sample fabricated at 700 °C as a function of time. From measured data, the generated voltage can be plotted versus the temperature difference, as shown in Fig. 2b.

The Seebeck coefficients of the fabricated samples, estimated by fitting the experimental data with a linear function as predicted by (1) and deriving the slope of the fitting line, are reported in Table 1. The sign of the measured thermoelectric coefficients is negative (positive) for ZnO (CuO) as expected for n-type (p-type) semiconductors. The experimental results are in agreement with recently reported values of Seebeck coefficient for ZnO nanostructures [6] and CuO thin film [7].

Figure 3a shows the trends of the applied temperature difference ΔT and the thermoelectric voltage ΔV versus time for the thermoelectric generator. The

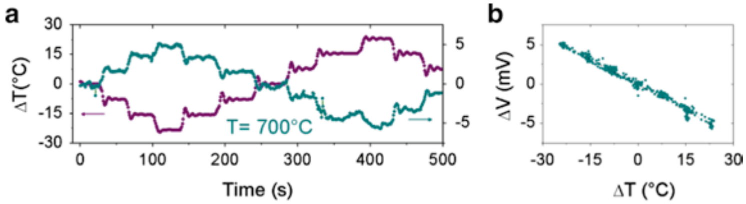

Fig. 2 (**a**) Trends of the applied temperature difference ΔT and the thermoelectric voltage ΔV versus time and (**b**) the voltage ΔV versus the applied temperature difference ΔT for the ZnO sample fabricated at 700 °C

Table 1 Measured Seebeck coefficients of the fabricated ZnO and CuO nanowire samples

Material	Deposition temperature (°C)	Seebeck coefficient α_m (mV/°C)
ZnO	700	–0.19
	870	–0.11
	1,070	–0.10
CuO	250	+0.82
	400	+0.43

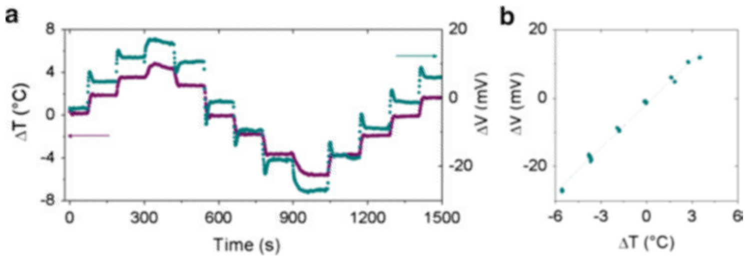

Fig. 3 (**a**) Trends of applied temperature difference ΔT and the voltage ΔV versus the time and (**b**) the generated voltage ΔV versus the applied temperature difference ΔT for the TEG

thermoelectric coefficient of the TEG has been estimated by linear fitting of the experimental data (Fig. 3b) and results of about 4 mV/°C; therefore, a single nanostructured ZnO–CuO thermocouple exhibits a Seebeck coefficient of about 0.8 mV/°C. The experimental data suggest that TEG based on the ZnO–CuO system could be investigated to supply low-power sensors and microsystems.

5 Conclusions

ZnO and CuO nanowire bundles have been deposited by thermal techniques and investigated for energy-harvesting applications by measuring Seebeck coefficient. A planar thermoelectric device based on five ZnO–CuO nanostructured thermocouples has been fabricated. Experimental data confirm the feasibility of fabricating planar thermoelectric generators for power generation based on ZnO and CuO nanowires deposited via shadow masks.

Acknowledgments Authors gratefully acknowledge partial financial support by the IIT, Project Seed 2009 “Metal oxide NANOwires as efficient high-temperature THERmoelectric Materials (NANOTHER).”

References

1. A. Vomiero, I. Concina, E. Comini, C. Soldano, M. Ferroni, G. Faglia, G. Sberveglieri, One-dimensional nanostructured oxides for thermoelectric applications and excitonic solar cells, Nano Energy, **1** (3), 372–390 (2012).
2. E. Comini, Metal oxide nano-crystals for gas sensing, Analytica Chimica Acta, **568** (1–2), 28–40 (2006).
3. D. Zappa, E. Comini, R. Zamani, J. Arbiol, J.R. Morante, G. Sberveglieri, Copper oxide nanowires prepared by thermal oxidation for chemical sensing, Procedia Engineering, **25**, 753–756 (2011).
4. S. Dalola, G. Faglia, E. Comini, M. Ferroni, C. Soldano, D. Zappa, V. Ferrari, G. Sberveglieri, Seebeck effect in ZnO nanowires for micropower generation, Procedia Engineering **25**, 1481–1484 (2011).
5. S. O. Kasap, Principles of electronic materials and devices, 2nd edition, McGraw Hill, New York (2005).
6. Y. Kinemuchi, M. Mikami, K. Kobayashi, K. Watari, Y. Hotta, Thermoelectric Properties of Nanograined ZnO, Journal of Electronic Materials, **39** (9), 2059–2063 (2009).
7. M Muhibbullah, M. O. Hakim, M.G.M Choudhury, Studies on Seebeck effect in spray deposited CuO thin film on glass substrate, Thin Solid Films, 423 (1), 103–107 (2003).

Piezopolymer Interdigital Transducers for a Structural Health Monitoring System

L. Capineri, A. Bulletti, M. Calzolai, and D. Francesconi

1 PPTs Fabrication Characteristics

The flexible piezopolymer transducers made with thin 100 μm PVDF film were proposed by the authors in previous works [1–3].

The proposed technology uses an array of transducers which can be designed to excite particular types of ultrasonic Lamb waves in laminate materials (metallic or composite). The finger to finger distance of interdigital electrode patterns determines the central wavelength of the transducer (λ) and then the corresponding Lamb waves mode. The piezoelectric polymer film can operate in a range of temperature (−80 to +60 °C) that is broader than that of ceramic transducers. Furthermore, the high mechanical compliance makes it adaptable to curved surfaces. A laser-based microfabrication design process can be tuned for efficient excitation and reception of selected Lamb waves. This property depends on the characteristics of laminate material and defect types. In our case we adopted 8 mm finger distance and four pairs of electrodes (see Fig. 1). Permanently glued on the vessel surface, a series of PZTs (Acellent Technologies, Inc., Sunnyvale, CA) used during previous tests is still present.

The piezopolymer interdigital transducers have been characterized at low temperature (−80 °C) and high temperature (+60 °C) showing no significant change of behavior, confirming that they can operate in the temperature range required for space application. Also levels of driving voltages and excitation burst frequency have been selected depending on the monitored medium. Because of the lower

L. Capineri (✉) • A. Bulletti • M. Calzolai
Department of Information Engineering, University of Florence,
Via S. Marta 3, 50139 Florence, Italy
e-mail: lorenzo.capineri@unifi.it

D. Francesconi
Thales Alenia Space Italia S.p.A, Strada Antica di Collegno 253, 10146 Torino, Italy

C. Di Natale et al. (eds.), *Sensors and Microsystems: Proceedings of the 17th National Conference, Brescia, Italy, 5-7 February 2013*, Lecture Notes in Electrical Engineering 268,
DOI 10.1007/978-3-319-00684-0_2,

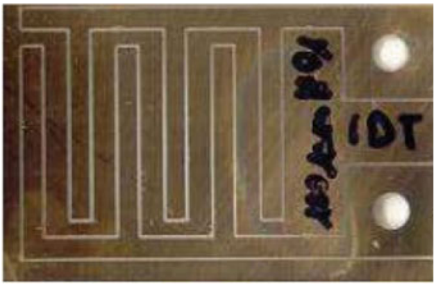

Fig. 1 The fabricated interdigital PPT made with thin 100 μm-thick PVDF film with $\lambda = 8$ mm. The two holes ($\phi = 2$ mm) are used for cables connection. Dimensions 26 mm × 37 mm

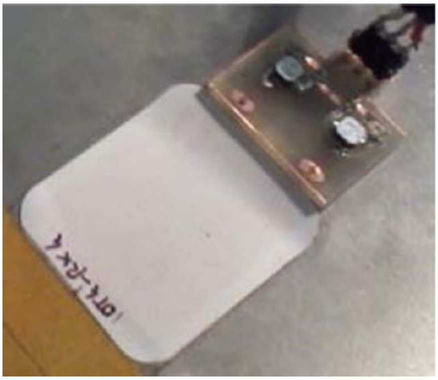

Fig. 2 Interdigital PPT with protective adhesive cover and the matching network designed. Implementation of the Piezopolymer Transducers Network

Fig. 3 Programmable acquisition system for active SHM on COPV with interdigital PPTs network

efficiency of PVDF with respect to PZT, higher voltages are necessary to drive the IDT transducers starting from low-voltage (±12 V) integrated driven circuit. Voltages up to 150 Vpp are obtained by designed matching networks (see Fig. 2).

All operations have been carried out with the scope of testing a piezopolymer transducers (PPTs) network applied on the surface of a scaled model of a carbon composite overwrapped pressurized vessel (COPV) to proof its efficiency for the localization of artificially induced damages on the COPV surface (see Fig. 3).

PPTs network has been designed for the wavelength $\lambda = 8$ mm, assembled on matching network designed connected to the receiving electronics. Adhesion of the sensors to the COPV surface is assured by smoothing with sandpaper and then degreasing with isopropyl alcohol the vessel surface. Then 8 PPTs (4 for the transmission Tx and 4 for the detection Rx) are installed on the vessel surface to investigate a portion of the cylindrical surface.

The chosen configuration (4+4 PPTs at 180 mm of distance spread along 180 mm depending on the defect characteristic and dimension) allows the acquisition of data along the paths between all possible pairs of transmitting and receiving transducers with a good signal-noise ratio.

2 Experimental Tests

A developed electronic system is programmed for the selection of multiple couples of pitch and catch PPTs and for the acquisition of relevant data. Front-end electronics has been designed and optimized for high signal-to-noise ratio taking into account the low power space requirements. The system includes also dedicated software that is developed to process off-line signals up to 8×8 different pairs of transducers for detecting both the damaged area and the size of the damage. The developed software interface controls the experiment and evaluates a damage index (DI) both in no damaged and damaged conditions and finally shows a colored scale image connected to the levels of probability of the presence of the damage.

Algorithm development for damaged area detection includes:

- The definition of signal paths from transmitter to the receiver
- The definition of excitation signal parameters
- The definition of artificially induced damages (drops of gel of 3 cm^2 size)
- The definition of Matlab routine managing the acquired signals of different paths before the DI calculation
- The calculation of DI based on the difference of both shape and amplitude of two acquired signals across the same path in undamaged and damaged conditions

Different artificial defects have been detected successfully by signal processing with the developed laboratory system: defects with area of about 3 cm^2 made by an ultrasonic gel drop on the surface of COPV have been detected successfully by using two arrays of four transmitters and four receivers placed at a distance of 180 mm. The antisymmetric A_0 mode at 220 kHz has been used to scan the area. The damage index image is shown in Fig. 4 corresponding to 1 for no defect and 0 for strong defect (no signals received).

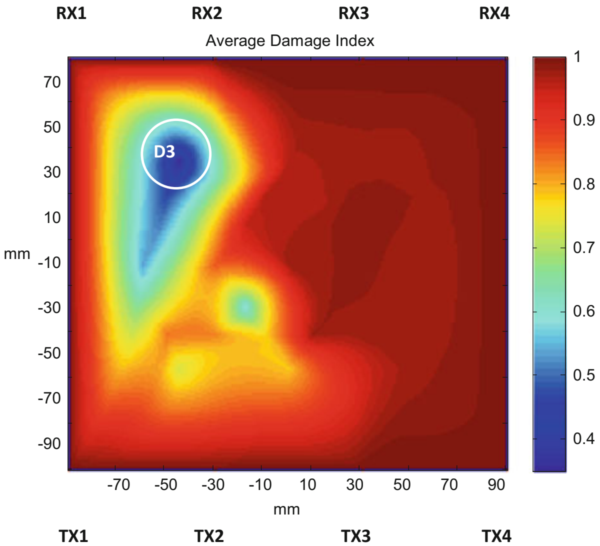

Fig. 4 Image of damage index distribution of the investigation area on COPV with defect D3 with real position ($x = -45°$; $y = +45°$)

References

1. L. Capineri, A. Gallai, L. Masotti, M. Materassi, "Design criteria and manufacturing technology of Piezo-polymer transducer arrays for acoustic guided waves detection", Ultrasonics Symposium, 2002. Proceedings. 2002 IEEE, Volume: 1, 8–11 Oct. 2002, pp. 857–860
2. F. Bellan, A. Bulletti, L. Capineri, L. Masotti, G. G. Yaralioglu, F. Levent Degertekin, B. T. Khuri-Yakub, "A new design and manufacturing process for embedded Lamb waves interdigital transducers based on piezopolymer film", Sensors and Actuators A 123–124 (2005) 379–387
3. F. Bellan, A. Bulletti, L. Capineri, A. Cassigoli, L. Masotti, O. Occhiolini, F. Guasti,, E. Rosi, "Review of non destructive testing techniques for composites materials and new applications ", Proceedings of The 10th Italian Conference on Sensors and Microsystems, Firenze, Italy, 15–17 February, 2005, World Scientific Publ. Pte. Ltd., Singapore Co., pp. 618–623

Noise and Performance of Magnetic Nanosensor Based on Superconducting Quantum Interference Device

C. Granata, R. Russo, E. Esposito, S. Rombetto, and A. Vettoliere

1 Introduction

The nano superconducting quantum interference device (nanoSQUID) is a powerful tool to study the magnetic properties of the nanoparticles at a microscopic level [1–7]. In fact, in the recent years, it has been shown that the magnetic response of nano-objects (nanoparticles, nanobead, small cluster of molecules) can be effectively measured by using a nanoSQUID [8, 9]. Typically, a dc nanoSQUID consists of a square loop having a side length less than 1 μm interrupted by two nanometric niobium constrictions (Dayem bridges) [2–4]. A small capture area improves the magnetic coupling between the SQUID and the nano-object under investigation allowing to obtain a sensitivity as high as few tens of Bohr magnetons per unit bandwidth [2–4]. In this paper, the design, the fabrication, and the characterization of hysteretic nanoSQUIDs based on Dayem nanobridges are reported. The effectiveness of such devices to measure magnetization and relaxation of iron oxide nanoparticles having a mean size ~8 nm demonstrated that our nano-devices are useful tools for nanomagnetism investigation.

2 Sensor Design and Characterization

We have designed and fabricated nanoSQUIDs consisting of a square hole with an inner side length of 0.75 μm, a width of 0.2 μm, and two Dayem bridges 120 nm long and 80 nm wide. We have used a configuration where the bias leads are

C. Granata (✉) • R. Russo • E. Esposito • S. Rombetto • A. Vettoliere
Istituto di Cibernetica "E. Caianiello" del Consiglio Nazionale
delle Ricerche, 80078 Pozzuoli, Napoli, Italy
e-mail: c.granata@cib.na.cnr.it

C. Di Natale et al. (eds.), *Sensors and Microsystems: Proceedings of the 17th National Conference, Brescia, Italy, 5-7 February 2013*, Lecture Notes in Electrical Engineering 268,
DOI 10.1007/978-3-319-00684-0_3,

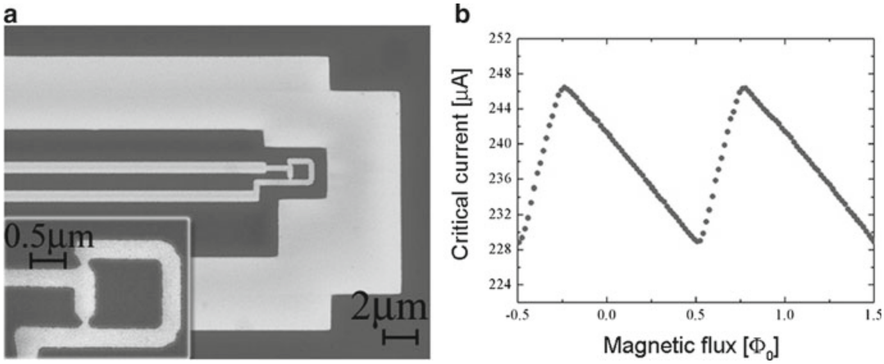

Fig. 1 (**a**) Scanning electron micrograph of a nanoSQUIDs in an asymmetric configuration. The integrated coil allows an effective modulation/calibration of the device. (**b**) Critical currents as a function of the external magnetic flux measured at $T = 4.2$ K

asymmetric with respect to the loop which corresponds to an inductance loop asymmetry. As we will show in the experimental results, such a configuration allows us to improve the critical current responsivity. A superconducting integrated coil located very close to the device allows to tune and set the optimal working point of the sensor (Fig. 1a).

The fabrication process is based on electron-beam lithography (EBL) process, which can directly pattern two-dimensional nanostructures on a high-resolution positive-tone polymethyl methacrylate (PMMA) electron-beam resist, spin-coated on a standard silicon wafer, used as substrate [9]. The EBL was used to pattern both the SQUID and an integrated coil into PMMA. A 20-nm-thick Nb film was deposited by dc magnetron sputtering in an ultra high-vacuum system with a base pressure of 10^{-8} mbar. A simple lift-off procedure is employed to obtain the SQUIDs and the related coil. A layer of flowable oxide (Fox-22 DOWCorning) is finally spin coated to obtain a passivation layer. The nanosensors have been characterized in liquid helium ($T = 4.2$ K) in a cryoperm magnetic shield using a low noise read-out electronic. In Fig. 2b, the I–Φ characteristic measured at $T = 4.2$ K has been reported. There is an appreciable increase of the curve slope on the steeper side of the characteristic, leading to an increase of the current sensitivity. As evaluated from the figure, the slope ratio between the steepest and the smoothest side is more than a factor three.

The magnetic flux resolution is given by $\Phi_N = \Delta I_{CN}/I\Phi$, where ΔI_{CN} is the minimum critical current difference detectable which depends on the critical current values and $I\Phi = \partial I_c/\partial \Phi_e$ is the magnetic flux to critical current transfer coefficient. For typical I_C value of 100–200 μA, ΔI_{CN} is about 0.01 μA, and considering a maximum $I\Phi$ of about 90 μA/Φ_0 for the asymmetric configuration (Fig. 1b), a magnetic flux resolution of 0.1 mΦ_0 can be estimated.

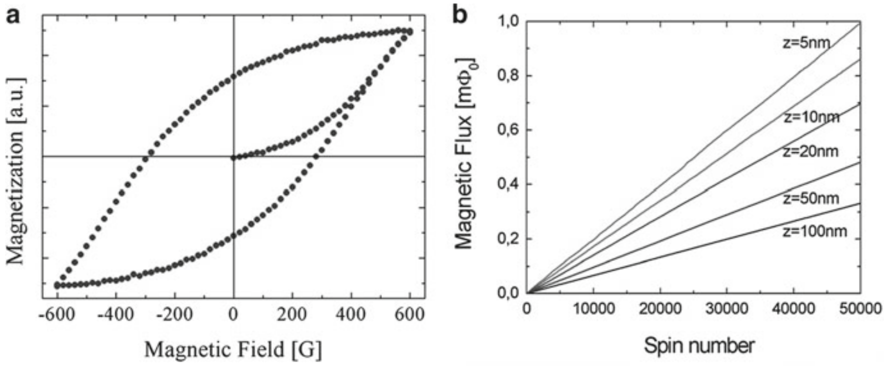

Fig. 2 (**a**) Field dependence of magnetization for 8-nm magnetic nanoparticles (*blue dots*) measured at $T = 4.2$ K by using a nanoSQUID. (**b**) Magnetic flux produced by a spin cluster as a function of the spin number, located within the SQUID hole at different distance z from the sensor plane. The overall magnetic flux has been obtained by summing up the flux contributions of each spin

3 Magnetization Measurement

Magnetization measurement relative to magnetite (Fe_3O_4) nanoparticles having a diameter of 8 nm has been performed. The measurement is obtained by measuring the critical current variation due to the change in the magnetic flux threading the SQUID loop. The experimental setup employed to perform these measurements is well described elsewhere [9]. The excitation field is provided by a solenoid coil able to produce a uniform magnetic field in the plane of the nanosensor of about 800 G, while a suitable feedback circuit provides the linearization of the nanoSQUID output. In this configuration, only the magnetic field arising from the nanoparticles will be measured, because the SQUID is sensitive only to the magnetic field normal to the capture area.

The nanoparticles were dispersed in hexane with a concentration of 6 mg/ml. A single drop of the solution of about 10 ml was left to dry on the chip (1 cm^2) leaving the nanoparticles stuck on the chip due to Van der Waals force. Supposing a uniform distribution of the solution on the chip, the mass of iron oxide in the active area of the sensor (0.5 μm^2) was about 0.3 pg corresponding to 10^4–10^5 nanoparticles [9]. In Fig. 2a, magnetic field dependence of the magnetization relative to Fe_3O_4 nanoparticles for a sweep magnetic field ranging from −600 to 600 G and measured at $T = 4.2$ K is reported. The sigmoid shape of the virgin curve at low magnetic field suggests the presence of dipole–dipole interparticle interactions which tend to resist to the magnetization process. The hysteresis indicates ferromagnetic features which are also present for lower field sweeps, suggesting that at $T = 4.2$, the magnetic nanoparticles under investigation are well below the blocking temperature. Unfortunately, the available magnetic field did not allow us to observe saturation, so only a minor loop have been recorded. The coercive field of such a loop is about 290 G.

By using the numerical calculations reported in ref. [10], we have computed the magnetic flux produced by a cluster of elementary magnetic moment (Bohr magnetons, $\mu_B = 9.3 \times 10^{-24}$ J/T), located within the SQUID hole at different distance from the sensor plane (Fig. 2b). Since the maximum SQUID output relative to the reported magnetization curve is about 1 Φ_0 and assuming a distance from the nanoparticles and the sensor plane of 10–100 nm, we have approximately estimated from Fig. 2b a value of the total magnetic moment of $(0.6–1.7) \times 10^8 \mu_B$ ($0.6–1.6 \times 10^{-12}$ emu) corresponding to (2–5) emu/g which is a reasonable value since the typical values of the magnetization at the saturation field (few *T*) reported in the literature are few tens of emu/g.

4 Conclusions

Low noise magnetic nanosensor based on Dayem bridge SQUID has been employed for the measurements of nanoparticles magnetization. A magnetic flux sensitivity of about 10^{-4} Φ_0 has been obtained by using an asymmetric nanoSQUID configuration. The sensor has been used in a hysteretic mode with suitable read-out scheme which has allowed to linearize the SQUID response. The magnetization measurements on iron oxide nanoparticles have shown an evident magnetic hysteresis indicating a blocking temperature well above 4.2 K. These results are very encouraging in view of a wide use of nanoSQUIDs for the nanomagnetism investigations.

References

1. J.P. Cleuziou, W.Wensdorfer, V. Bouchiat, T. Ondarcuchu, M. Monthioux, “Carbon nanotube superconducting quantum interference device” Nature Nanotech. **1**, 53–59 (2006).
2. A.G.P. Troeman, H. Derking, B. Boerger, J. Pleikies, D. Veldhuis, H. Hilgenkamp, “NanoSQUIDs Based on Niobium Constrictions” Nano Lett. **7**, 2152–2156 (2007).
3. C. Granata, E. Esposito, A. Vettoliere, L. Petti, M. Russo, “An integrated superconductive magnetic nanosensor for high-sensitivity nanoscale applications” Nanotechnology, **19**, 275501–275506 (2008).
4. L.Hao, J.C. Macfarlane, J.C. Gallop, D. Cox, J. Beyer, D. Drung, T. Schuring, “Measurement and noise performance of nano-superconducting-quantum interference devices fabricated by focused ion beam” Appl. Phys. Lett. **92**, (192507–102509) (2008).
5. W. Wernsdorfer, “From micro-to-nano-SQUIDs: applications to nanomagnetism” Supercond. Sci. Technol. **22**, 064013 1–13 (2009).
6. C. Granata, A. Vettoliere, R. Russo, E.Esposito, M.Russo, B. Ruggiero,” Supercurrent decay in nano-superconducting quantum interference devices for intrinsic magnetic flux resolution” Appl. Phys. Lett. **94**, 062503 1–3 (2009).
7. C. Granata. A. Vettoliere, M. Russo and B. Ruggiero, “Noise theory of dc nano-SQUIDs based on Dayem nanobridges” Phys Rev. **B 84**, 224516 1–7 (2011).

8. L. Hao, C. Aßmann, J. C. Gallop, D. Cox, F. Ruede, O. Kazakova, P. Josephs-Franks, D. Drung, and Th. Schurig,"Detection of single magnetic nanobead with a nano-superconducting quantum interference device", Appl. Phys. Lett. **98**, 092504 1–3 (2011).
9. R. Russo, C. Granata, E. Esposito, D. Peddis, C. Cannas and A. Vettoliere, "Nanoparticle magnetization measurements by a high sensitive nano-superconducting quantum interference device", Appl. Phys. Lett. **101**, 122601 1–3 (2012).
10. C. Granata, A. Vettoliere, P. Walke, C. Nappi and M. Russo, Performance of nano superconducting quantum interference devices for small spin cluster detection", J. Appl. Phys. **106**, 023925 1–5 (2009).

Nonintrusive IR Sensor for Real-Time Measurements of Gas Turbine Inlet Temperature

E. Golinelli, S. Musazzi, U. Perini, and F. Barberis

1 Introduction

Turbine inlet temperature (TIT) is a critical parameter of gas turbine systems influencing both material and coating lifetime of turbines as well as their efficiency. For this reason, online TIT monitoring systems are highly desirable since they would allow both to foresee with higher reliability the residual life of the most critical hot parts of the turbine and, at the same time, to maximize the gas temperature (although it should remain within the limits for materials and coatings operation) so as to increase the gas turbine overall efficiency.

Unfortunately, at present, there are no available methods to accurately measure this parameter on operating plants. For these reasons, we have developed a temperature sensor based on spectroscopic photometric measurements of the infrared radiation emitted in a selected wavelength band by the CO_2 molecules of the combustion gases. The sensor has been designed to provide online and in real-time measurements of the average gas temperature on a plant section transversal to the gas flow. The developed prototype is mechanically robust and thermally resistant to withstand typical operating conditions of industrial gas turbines. It has been tested both at laboratory level in controlled stable conditions and on a full-scale combustor test bed simulating the behavior of real gas turbine machine.

2 Principle of Operation

The measuring technique is a sort of emission-absorption pyrometry like the one utilized in nonreacting gas mixtures with negligible reflectivity [1]. The measured quantity is the grey body spectral irradiance $H(\lambda,T)$ defined by the product of the

E. Golinelli • S. Musazzi (✉) • U. Perini • F. Barberis
Ricerca sul Sistema Energetico—RSE, Via Rubattino 54, 20134 Milano, Italy
e-mail: sergio.musazzi@rse-web.it

C. Di Natale et al. (eds.), *Sensors and Microsystems: Proceedings of the 17th National Conference, Brescia, Italy, 5-7 February 2013*, Lecture Notes in Electrical Engineering 268,
DOI 10.1007/978-3-319-00684-0_4,